The role of flow shear in the ballooning stability of tokamak transport barriers

A. J. Webster,[a] H. R. Wilson, and A. M. M. Scaife
UKAEA/Euratom Fusion Association, Culham Science Centre, Abingdon, Oxfordshire, OX14 3DB, United Kingdom

(Received 24 October 2003; accepted 21 January 2004; published online 16 April 2004)

A tokamak's economic performance is strongly affected by the plasma pressure that it may sustain, which in turn is limited by the maximum pressure gradients that may be supported. Ballooning modes are typically driven unstable by increasing the pressure gradient, and because they can radially extend across many rational surfaces, they can seriously reduce a plasma's energy confinement. Here an eigenmode formulation is used to study the stability of ballooning modes in internal transport barriers (''ITBs''), in which very strong pressure gradients and flow shears may be found. This extends previous studies that used an ''eikonal'' formulation, as it enables the study of: ballooning modes with a finite toroidal mode-number n (finite wavelength perpendicular to the magnetic field), to find new solution branches, to obtain the eigenmode structures, and to investigate the effects of a radially varying equilibrium. The structure of a finite n ballooning mode in flow shear is found to be significantly affected by a radially varying equilibrium, and at low flow shears the growth rates are increased above those of modes studied in the limit of $n\rightarrow\infty$. The different solution branches can couple as the flow shear is increased, leading to a pair of asymmetric mode structures with complex conjugate growth rates. These effects are shown to be a consequence of the mode trying to localize at the most unstable radial location, and its desire to rotate with the flow. In addition, closer to marginal stability a sufficiently strong flow-shear can (at least for some cases), destabilize a previously stable mode. [DOI: 10.1063/1.1687724]

I. INTRODUCTION

Ideal magnetohydrodynamics (''MHD''), predicts that the most unstable short wavelength (high toroidal mode number) instabilities are ''ballooning modes,'' instabilities that minimize the bending of magnetic field lines.[1] These modes are well understood for plasmas without flows, and are most likely to be unstable in tokamak plasmas with high pressure gradients.[2–5] The highest pressure gradients are found in transport barriers, as are strong flow-shears, hence the need to understand how flow shear affects the structure and stability of ballooning modes.[6,7]

In the absence of flow shear, ballooning modes are studied with an eikonal formalism and a ''ballooning expansion.''[3] The ballooning expansion enables the construction of a periodic perturbation $\hat{\boldsymbol{\xi}}$ from a nonperiodic one $\boldsymbol{\xi}$, with

$$\hat{\boldsymbol{\xi}}(\chi,\psi,\phi)=\sum_{N=-\infty}^{\infty}\boldsymbol{\xi}(\chi-2\pi N,\psi,\phi) \tag{1}$$

for which the periodicity condition $\hat{\boldsymbol{\xi}}(\chi+2\pi)=\hat{\boldsymbol{\xi}}(\chi)$, is replaced by the boundary condition that $\boldsymbol{\xi}(\chi\rightarrow\pm\infty)\rightarrow 0$. The ballooning expansion enables us to subsequently use the eikonal formulation

$$\boldsymbol{\xi}=\mathbf{F}(\chi,\psi)e^{inS(\psi,\chi,\phi)} \tag{2}$$

with derivatives on S parallel to the magnetic field $\mathbf{B}$, being $\mathbf{B}.\nabla S=0$, and without needing S to be periodic in χ.

The usual choice for the eikonal is

$$S=-\phi+\int_{\chi_0}^{\chi}\nu d\chi' \tag{3}$$

with $\nu(\chi,\psi)$ being a measure of the local pitch of the field lines.[3] However at lowest order in $1/n$, a nonzero toroidal flow $\mathbf{v}_0$ leads to convective derivatives $\mathbf{v}_0.\nabla e^{inS}$ that diverge as n tends to infinity. So the most unstable high-n perturbations must now minimize both the magnetic field-line bending and the stream-line bending of the plasma flow. A modified eikonal that reflects this uses the fact that the $\mathbf{v}_0.\nabla$ operator occurs in conjunction with the $\partial/\partial t$ operator, so that both

$$\left(\frac{\partial}{\partial t}+\mathbf{v}_0.\nabla\right)\mathbf{F}(\psi,\chi)e^{inS(\psi,\chi,t)}=e^{inS(\psi,\chi,t)}\frac{\partial\mathbf{F}}{\partial t} \tag{4}$$

and

$$\mathbf{B}.\nabla\{\mathbf{F}(\psi,\chi,t)e^{inS(\psi,\chi,t)}\}=e^{inS(\psi,\chi,t)}\frac{1}{J}\frac{\partial\mathbf{F}}{\partial\chi} \tag{5}$$

with $\partial\mathbf{F}/\partial t$ and $\partial\mathbf{F}/\partial\chi$ of order 1, and J the Jacobian of the orthogonal (ψ,χ,ϕ) coordinate system.[3] For a toroidally axisymmetric flow, the eikonal used is[8]

$$S(\psi,\chi,t)=\left(-\phi+\int_{\chi_0}^{\chi}\nu d\chi'+\Omega t\right) \tag{6}$$

with $\Omega(\psi)$ being a radially dependent angular toroidal flow

[a]Electronic mail: Anthony.Webster@ukaea.org.uk

for which $\mathbf{v}_0=\Omega(\psi)R\mathbf{e}_\phi$, and where R is the major radius. The shortcoming of using this representation for a linearized stability analysis, is that radial derivatives on S lead to terms in $\Omega' t$. So despite being linearized MHD, the time dependence is not simply $\boldsymbol{\xi}\sim e^{\gamma t}$. Thus the problem involves time as an extra coordinate, and stability is determined by the solution of 4 coupled first-order 2D partial differential equations.[9] This contrasts with zero flow-shear for which as $n\to\infty$, the problem reduces to a 1D second order ordinary differential equation in ballooning space.[2,3]

Previous authors[9,10] have used this eikonal formalism (in the $n\to\infty$ limit) to study ballooning stability in flow shear, by using an initial value code to solve the equations. In particular, Miller *et al.*[9] have applied the method to study a circular-flux-surfaces ("s–α" type) model of the equilibrium, that includes toroidal flow. In that model, internal transport barriers ("ITBs") are represented by a narrow annular region with a strong flow-shear and a large gradient in the plasma pressure p. A low $\beta=2p/B^2$ ordering is also taken, where B^2 is the total magnetic field strength. This enabled the study to focus solely on the effects of flow shear, which they showed can stabilize ballooning modes. Furukawa *et al.*[10] have applied the same eikonal formalism to realistic, arbitrary aspect ratio tokamak geometries, finding qualitatively similar results.

Here we describe an eigenmode formalism that we use to study ballooning modes in a sheared plasma flow. The growth rate is determined as an eigenvalue, the eigenfunctions determine the mode structures, and the method enables us to study flow shear in a radially varying equilibrium (for finite n), and to discern multiple solution branches (in addition to the most unstable branch). We find that in the presence of a small though nonzero flow shear, the $n=\infty$ ballooning modes studied by Miller *et al.*[9] are more stable than the strictly zero flow-shear ballooning modes studied in Ref. 3; the latter having *larger* growth rates and *different* mode structures. This is explained in terms of the radially dependent equilibrium profile introducing a radial-dependence for the stability of ballooning modes, the flow-shear's tendency to narrow the mode envelope, and the modes desire to rotate with the flow. We also find that closer to marginal stability a sufficiently high flow shear can destabilise a previously stable mode; this was not observed in Ref. 9.

II. STABILITY ANALYSIS

We study the ITB model of Miller *et al.*,[9] with isothermal flux surfaces, an axisymmetric flow, and with centrifugal effects from the flow neglected but terms in the flow shear retained. For this model the equilibrium is determined by the usual Grad–Shafranov equation.[1]

The stability analysis starts by expressing the linearized MHD equations in terms of a single "force-balance" equation, projected in the $\mathbf{B}$, $\nabla\psi$, and $\mathbf{B}\wedge\nabla\psi$ directions. These equations are given in Ref. 11, as are further details of the following calculation. We then use the high-n ballooning mode ordering of $\mathbf{B}.\nabla\boldsymbol{\xi}\sim 1$, $\nabla\psi.\nabla\boldsymbol{\xi}\sim n$, and $\nabla\phi.\nabla\boldsymbol{\xi}\sim n$, to reduce the three original equations to two simpler ones. These are,

$$-\mathbf{B}.\nabla\left[\frac{1}{R^2B_p^2}\left[\left(\frac{R^2B_p^2}{B}\right)^2\partial_\psi^2+1\right]\mathbf{B}.\nabla F\right]-\hat{K}[p'F+pG]+\frac{\Gamma^2p}{c_s^2}\frac{1}{R^2B_p^2}\left[\frac{1}{\Gamma^2}\left(\frac{R^2B_p^2}{B}\right)^2\partial_\psi\Gamma^2\partial_\psi+1\right]F=0 \tag{7}$$

and

$$\mathbf{B}.\nabla\left[\frac{1}{B^2}\mathbf{B}.\nabla G\right]=\left(\frac{\Gamma^2}{c_s^2}\right)\left[\frac{(p+B^2)}{B^2}G+\hat{K}F\right] \tag{8}$$

with

$$\hat{K}\equiv\frac{1}{B^2}\left[\frac{\partial}{\partial\psi}(2p+B^2)+I\frac{\mathbf{B}.\nabla B^2}{B^2}\partial_\psi\right], \tag{9}$$

where we have written $\nabla\psi.\boldsymbol{\xi}=\Gamma F$ and $\nabla.\boldsymbol{\xi}=\Gamma G$, with $\Gamma=\gamma-in\Omega(\psi)$, and γ is the growth rate for which $\xi\sim e^{\gamma t}$, B_p is the poloidal magnetic field, R is the major radius, $\partial_\psi\sim(i/n)(\partial/\partial_\psi)$, and c_s is the sound speed.

A rapid radial coordinate $x=n(q_0-q)$ is used, in terms of which $in\Omega(x)=in\Omega_0-i(d\Omega/dq)x+O(1/n)$, where q is the safety factor and q_0 its value on a reference flux surface. The constant $in\Omega_0$ term is incorporated into a Doppler shifted growth rate, with γ replaced by $\gamma-in\Omega_0$ (where $\xi\sim e^{\gamma t}$), and Γ becomes $\Gamma=\gamma+i(d\Omega/dq)x$. So the explicit n dependence is removed from our leading order equations because equilibrium quantities change over a longer radial length-scale than the perturbation ξ, and by the incorporation of the constant frequency Ω_0 into a Doppler shifted growth rate.

Using the large-aspect-ratio model of Miller *et al.*,[9] and Fourier expanding in straight field-line coordinates θ, with $F=\Sigma_m u_m(x)\exp\{-in\phi+im\theta\}$ and $G=\Sigma_m g_m(x)\exp\{-in\phi+im\theta\}$ results in the leading order equations (in $1/n$),

$$\begin{aligned}0=&s^2\frac{d}{dx}\left[[(x-M)^2+\Gamma^2]\frac{du_m}{dx}\right]-[(x-M)^2+\Gamma^2]u_m\\&+\alpha\Bigg\{-\frac{s}{2}\frac{d}{dx}[[(x-M)^2+\Gamma^2](u_{m+1}-u_{m-1})]\\&-\frac{s}{2}[(x-M)^2+\Gamma^2+1]\frac{d}{dx}[u_{m+1}-u_{m-1}]\\&-s(x-M)\frac{d}{dx}[u_{m+1}+u_{m-1}]+\frac{1}{2}[u_{m+1}+u_{m-1}]\Bigg\}\\&-\frac{\alpha^2}{2}\Bigg\{[(x-M)^2+1+\Gamma^2]\left[u_m-\frac{1}{2}[u_{m+2}+u_{m-2}]\right]\\&-(x-M)[u_{m+2}-u_{m-2}]\Bigg\}-q^2\beta\Bigg\{+(g_{m-1}+g_{m+1})\\&-\alpha\left[g_m-\frac{1}{2}[g_{m-2}+g_{m+2}]\right]-s\frac{d}{dx}[g_{m+1}-g_{m-1}]\Bigg\}\end{aligned} \tag{10}$$

and

$$g_m=\left(\frac{\Gamma^2}{(x-M)^2+\Gamma^2}\right)\left\{(u_{m+1}+u_{m-1})-\alpha\left[u_m-\frac{1}{2}(u_{m+2}+u_{m-2})\right]-s\frac{d}{dx}(u_{m+1}-u_{m-1})\right\}. \tag{11}$$

The expansion used

$$\frac{1}{q}\int^{\chi}\nu d\chi'\simeq\theta,$$

$$\frac{\partial}{\partial\psi}\left[\frac{1}{q}\int^{\chi}\nu d\chi'\right]\simeq\left(\frac{-\alpha}{rRB_p}\right)\sin(\theta),$$

$$\frac{du_m}{d\psi}=-nq\frac{s}{rRB_p}\frac{du_m}{dx},$$

and

$$M\equiv m_0-m.$$

The equations are normalized such that $\Gamma(x)^2$ replaces $[\Gamma(x)^2R^2q^2/c_s^2](p/B^2)$, u_m replaces u_m/R^2B_p, with $s=(r/q)(dq/dr)$ and $\alpha=-(2r^2/RB_p^2)(dp/dr)$ being the usual normalized magnetic-shear and pressure-gradient parameters, respectively.[2]

For simplicity we consider the limit $\beta\ll 1$, $(d\Omega/dq)R/c_s\gg\sqrt{\beta}$, for which terms in the flow shear are retained while those in β may be neglected. In this limit we have,

$$\begin{aligned}s^2\frac{d}{dx}\left[[(x-M)^2+\Gamma^2]\frac{du_m}{dx}\right]&-[(x-M)^2+\Gamma^2]u_m+\alpha\\&\times\left\{-\frac{s}{2}\frac{d}{dx}[[(x-M)^2+\Gamma^2](u_{m+1}-u_{m-1})]\right.\\&-\frac{s}{2}[(x-M)^2+\Gamma^2+1]\frac{d}{dx}[u_{m+1}-u_{m-1}]-s(x-M)\\&\left.\times\frac{d}{dx}[u_{m+1}+u_{m-1}]+\frac{1}{2}[u_{m+1}+u_{m-1}]\right\}\\&-\frac{\alpha^2}{2}\left\{[(x-M)^2+1+\Gamma^2]\left[u_m-\frac{1}{2}[u_{m+2}+u_{m-2}]\right]\right.\\&\left.-(x-M)[u_{m+2}-u_{m-2}]\right\}=0\end{aligned} \tag{12}$$

as the equations that we solve for a range of m.

It is worth pointing out a few features of Eq. (12). First, the equilibrium parameters s, α, and $d\Omega/dq$ all correspond to the degree of shear of an equilibrium quantity. Second, the flow has been normalized such that $(\Omega Rq/c_s)\sqrt{p/B^2}=\Omega Rq/v_A$ is replaced by Ω, with the flow speed $v_0=\Omega R$ normalized with respect to the Alfvén velocity v_A. Finally, the flow shear solely appears through

$$\Gamma(x)=\gamma+i\frac{d\Omega}{dq}x \tag{13}$$

and we have taken

$$\xi\sim e^{\gamma t-in\phi}=e^{\mathrm{Re}(\gamma)t}e^{i(\mathrm{Im}(\gamma)t-n\phi)}. \tag{14}$$

So $\mathrm{Im}(\gamma)=0$ corresponds to zero mode rotation, and when $\mathrm{Im}(\gamma)+(d\Omega/dq)x_s=0$, the mode rotates with the flow's equilibrium rotation at the radial position $x=x_s$.

III. NUMERICAL METHOD FOR SOLVING THE EQUATIONS

Zero flow ballooning-theory,[3] indicates that a finite radial mode-width is not possible for constant equilibrium parameters s and α. Therefore we introduce slow equilibrium variations, taking the magnetic shear s as constant, but adopting a Gaussian pressure gradient profile

$$\alpha(x)=\alpha_0\exp\left[-\frac{a^2}{2}\frac{(x-x_0)^2}{n^2q_0^2s^2}\right], \tag{15}$$

where x is normalized to give an α profile in x space that corresponds to the α profile of a typical transport barrier in real space, with $a=r/\Delta r$ (r is the minor radius and Δr is the transport barrier width). Then Connor *et al.*[3] predict a radial mode-envelope that is centred on $x=x_0$, with a width in x-space that scales as $\Lambda\equiv\sqrt{nq/a}$, and a growth rate with an order $1/\Lambda^2$ correction to the $n=\infty$ growth rate γ_∞. The equations, which now depend weakly upon n, are solved with the boundary condition that the mode amplitudes tend to zero as $x\to\pm\infty$.

We note that by introducing a radially dependent α profile, we have introduced terms of order (x^2/n^2), that were previously considered negligible. Although not strictly rigorous, it is a simple and transparent way of incorporating the most important effect of the order $1/n$ terms; that is to break the zero flow-shear ballooning symmetry between rational surfaces. Without this, it is this equivalence between rational surfaces (and Fourier mode structures), that causes the ballooning mode to be of infinite radial extent.

Because in the absence of flow, the mode width in x space is proportional to Λ, the x coordinate must also extend over a distance proportional to Λ. Thus for fixed a, the finite x-domain of calculation imposes a maximum n that we can treat when the flow-shear is zero. To obtain the $n=\infty$ growth rate we must extrapolate in Λ, using $\gamma=\gamma_\infty-O(1/\Lambda^2)$.[3,12]

When there is zero flow-shear, each Fourier mode has its maximum amplitude at the radial position at which it minimizes the bending of the magnetic field lines. This radial position corresponds to the rational surface q, for which $m=nq$ and $x=M$, and because the mode width is proportional to Λ, we require of order Λ Fourier modes. So for a given Λ, the range of x and M must be sufficiently large that $u_m\to 0$ at the largest values of x and M.

We integrate the u_m from $x=0$ to $x=\pm\infty$ using a shooting method, with the boundary condition that $u_m=0$ as $x\to\pm\infty$. This is done by first writing

$$u_m(x)=\sum_j v_m^j(x)a_j, \tag{16}$$

where the $v_m^j(x)$ are a set of basis solutions with the boundary conditions of $v_m^j(0)=\delta_{mj}$ and $v_m^j(\pm\infty)=0$. Each $v_m^j(x)$ may be integrated in the positive and negative directions

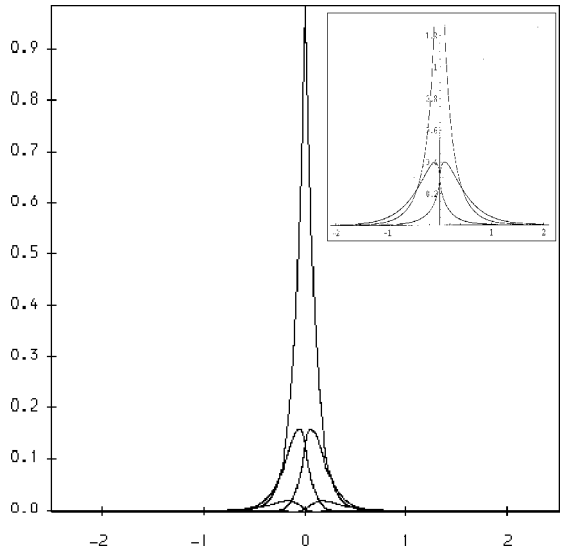

FIG. 1. Low magnetic shear: $s=0.1$, $\alpha=0.5$, and zero flow shear. The individual Fourier modes $u_m(x)$ are plotted in terms of the radial coordinate $x=m_0-nq$. Inset, the equivalent analytical calculation but with $s\sim\alpha\rightarrow 0$, at marginal stability (Ref. 14).

from $x=0$ to $x=\infty$ and $x=0$ to $x=-\infty$ (where in practice $x=\pm\infty$ means a sufficiently large value of x that our results are independent of it).

The coefficients a_j of Eq. (12) are determined from the requirement that the discretized version of Eq. (12) for the $u_m(x)$ must be satisfied at $x=0$. This requires $\mathbf{T}(\gamma).\mathbf{a}=\mathbf{0}$, where the elements of the matrix $\mathbf{T}$ depend on the numerically integrated values of $v_m^j(x)$ adjacent to $x=0$, which in turn depend on γ. The elements of $\mathbf{a}$ are the coefficients a_j in Eq. (16).

To solve $\mathbf{T}(\gamma).\mathbf{a}=\mathbf{0}$, we introduce the eigenvectors and eigenvalues λ_i and $\mathbf{e}_i$ for which $\mathbf{T}(\gamma)\mathbf{e}_i=\lambda_i\mathbf{e}_i$, and iterate γ until $\lambda_i(\gamma)=0$ for an $\mathbf{e}_i\neq 0$. Because $\lambda(\gamma)$ is complex, we search for zeros of $\lambda(\gamma)$ in the complex plane using the zero-finding program ZERINT,[13] tracking the eigenvalue λ with the largest real part. Searching different regions of the complex plane may lead to different solutions for γ, and the γ with the largest real part is the most unstable solution. In practice we usually start with a known solution and track it as we change a parameter such as flow shear. For example, a zero flow-shear solution can be tracked as the flow shear is increased (ensuring that at least initially, we are calculating the most unstable growth rate).

IV. RESULTS

Low magnetic shear and finite flow-shear are both characteristic properties of ITBs. Before we consider flow shear, we briefly investigate the effect of a low magnetic shear s, with $s=0.1$ and $\alpha=0.5$. The resulting mode structures are highly localized (Fig. 1), and are insensitive to changes in Λ. These surprising results agree with analytic calculations for $s\sim\alpha^2\rightarrow 0$, at marginal stability ($\gamma=0$),[14] Fig. 1(inset).

Next we consider flow shear, which radially localises the mode, even for $\Lambda=\infty$ and s of order 1. This is in agreement with approximate analytic calculations with $d\Omega/dq\ll 1$ and $\Lambda=\infty$, that suggest that the mode width scales as $\sim\sqrt{1/(d\Omega/dq)}$. So for finite flow shear we can take $\Lambda=\infty$ and directly compare our results with Miller *et al.*'s study of that limit. The results are in good agreement (Fig. 2). The radial envelope of the Fourier modes is symmetric [Figs. 3(a)–3(c)], and narrows as the flow shear is increased. Interestingly, at high flow-shears the mode envelopes appear self-similar in shape (though narrowed in width), and the growth rates are real throughout.

Figures 3(d)–3(f) shows the mode structures in the poloidal cross section. The modes are peaked on a radial surface $r=r_0$, for which the flow is zero. There is positive toroidal flow for $r>r_0$ and negative toroidal flow for $r<r_0$. Positive flow causes the mode to rotate clockwise relative to the zero flow mode, whereas negative flow causes anticlockwise rotation of the mode. The net effect is that the mode's peaks are elongated in the upper half of Figs. 3(d)–3(f), but narrowed in the lower half of the figure.

The poloidal shearing of the mode can be explained in terms of the the plasma flow convecting the magnetic field lines, with field lines convected in the $\pm\phi$ direction for positive flow and negative flow respectively. Figure 4 shows how the combination of the convection of the field lines and the nonzero field line pitch, causes the position at which field lines cut the poloidal plane to move upward or downward

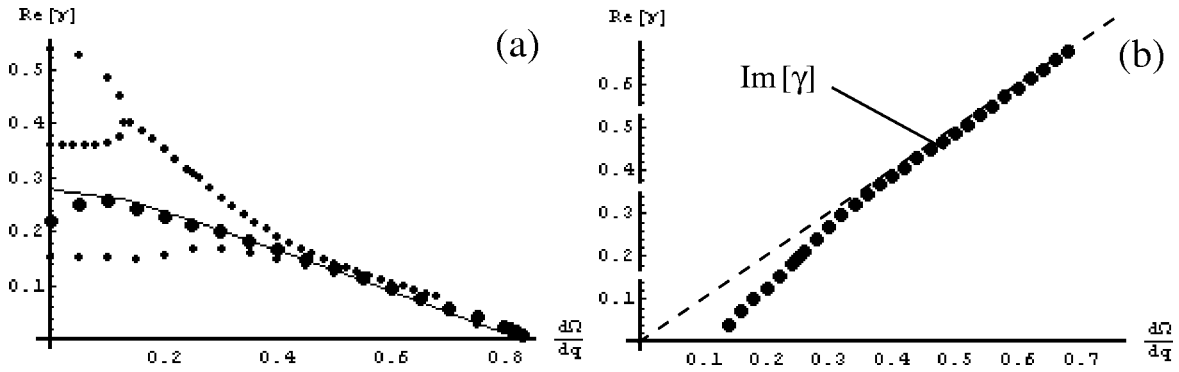

FIG. 2. The growth rate is plotted for $s=1$, $\alpha=2$, as the flow shear is increased. In (a) circles are for $\Lambda=\infty$, and agree well with calculations of Miller *et al.* (continuous line). The crosses in (a) are calculations for $\Lambda=1.35$, and show 3 solution branches, the top two of which coalesce as the flow shear is increased. After coalescence of the top two solution branches, there are two complex conjugate solutions, whose imaginary part is roughly proportional to $d\Omega/dq$ (b).

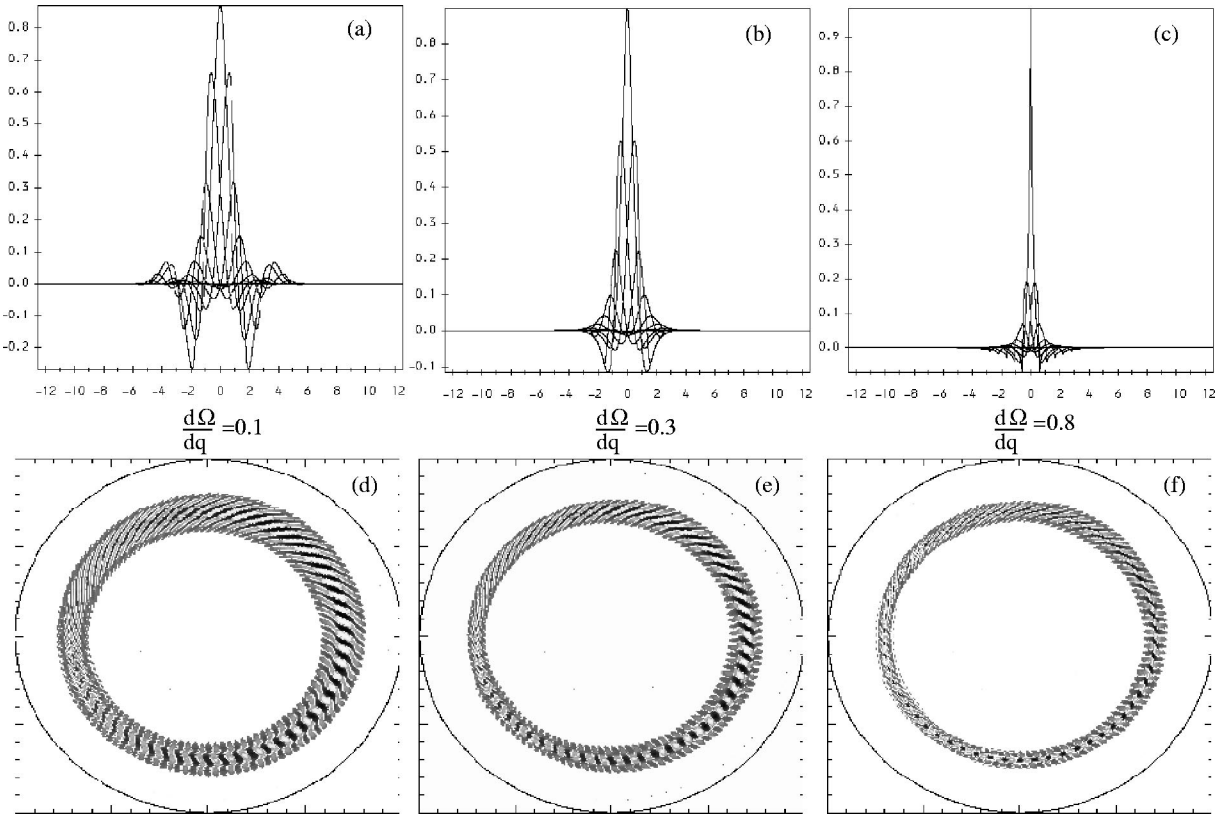

FIG. 3. (a)–(c) Plots of the individual Fourier mode amplitudes $u_m(x)$, for $s=1$, $\alpha=2$, $\Lambda=\infty$, and $d\Omega/dq=0.1$, 0.3, and 0.8, respectively. The corresponding plots in the lower half of the figure, (d)–(f), show poloidal cross sections for the amplitude of the perturbations. The intensity of the light and dark indicates the amplitude of the mode.

depending on the flow direction (and the field-line pitch). The result is a clockwise (positive flow) or anticlockwise (negative flow) rotation of the mode structure in the poloidal plane, shearing the mode with respect to the position of zero flow.

We turn now to finite Λ, taking $\Lambda=1.35$. For zero flow-shear there are 3 unstable modes (Fig. 2). These modes correspond to the three most unstable solutions of the mode envelope equation [Eq. (36) of Ref. 3], and their Fourier mode structures are shown in Fig. 5. As the flow shear is increased the two most unstable branches of Fig. 2 coalesce. After coalescence, γ becomes complex and there exist two complex conjugate solutions, whose Fourier mode structures are asymmetric, but mirror images of one another [Fig. 6(b)]. It is noticeable that at low flow shears the finite Λ growth rates are much larger than those for $\Lambda=\infty$. This is partially explained by the results of analytic calculations with low flow shears and $n\to\infty$. These calculate the growth rate in terms of the zero-flow growth rate $\gamma_0(\theta_0)$, where θ_0 is determined by the higher order theory.[3] For strictly zero flow-shear, θ_0 should be chosen to maximize $\gamma(\theta_0)$.[3] However for finite but infinitesimally small flow shear, one averages over θ_0: $\gamma=(1/2\pi)\oint\gamma_0(\theta_0)d\theta_0$.[15] The result is that for $n\to\infty$, there is an abrupt drop in γ as flow shear is increased from zero.

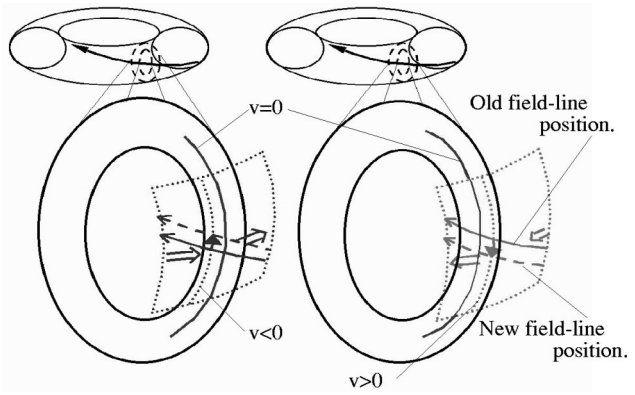

FIG. 4. The figure shows the convection of field lines by the plasma flow at radial positions for which the flow is positive and negative respectively. Because the field line has a nonzero pitch (q is finite), the position at which it cuts the poloidal plane moves up (or down) for positive (or negative) flow, respectively.

At finite n, Fig. 2 shows that for $\Lambda=1.35$ the growth rates tend to those of $\Lambda=\infty$ provided that $d\Omega/dq$ is sufficiently large. The value of $d\Omega/dq$ at which the $\Lambda=\infty$ and the finite Λ results converge, is smaller as Λ is increased, suggesting that the radial α variations are suppressing the averaging of $\gamma(\theta_0)$. The mode structures in poloidal cross section for $\Lambda=1.35$, show the mode's peak being torn into two pieces [Fig. 6(b)], unlike for $\Lambda=\infty$ where the peak remains intact but its edges are torn.

It is worthwhile to emphasize the differences between $n=\infty$ and finite n, for the different cases of arbitrarily small,

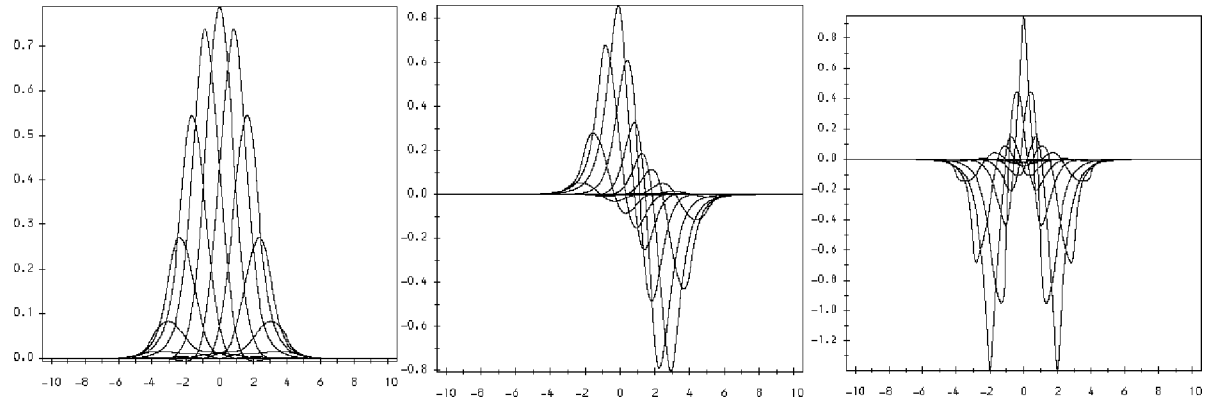

FIG. 5. $s=1$, $\alpha=2$, and zero flow shear: 3 solution branches may be found, with the usual ballooning mode solution (leftmost) being the most unstable, and the most stable being furthest right. These solutions are thought to be related to the 3 most unstable solutions of the conventional ballooning mode envelope equation (Ref. 3).

and strictly *zero* flow-shear. When the flow shear is strictly zero, the most unstable finite-n growth rate is always less than the $n=\infty$ growth rate (that in our eigenmode formalism, is obtained by extrapolating in $1/\Lambda^2=a/nq$). Things are very different for arbitrarily small flow-shears however. Once the flow shear is nonzero, the $n=\infty$ growth rate is reduced from $\max[\gamma(\theta_0)]$ to $(1/2\pi)\oint\gamma(\theta_0)d\theta_0$. However we find this *does not* happen when Λ is finite, for which substantial flow shears are required to significantly reduce the growth rate. Hence for arbitrarily small flow shears, the finite-n growth rates are *larger* than the $n=\infty$ ones.

So why has finite Λ resulted in radially asymmetric mode structures and complex conjugate growth rates? The behavior can be explained in terms of the mode trying to localize at the most unstable radial position, and subsequently trying to rotate with the flow. Figure 7 for the growth rate $\gamma(\alpha)$, shows that for $s=1$, $d\Omega/dq=0$ the most unstable value of α is $\alpha\simeq 1.7$.[16] We have assumed a Gaussian profile

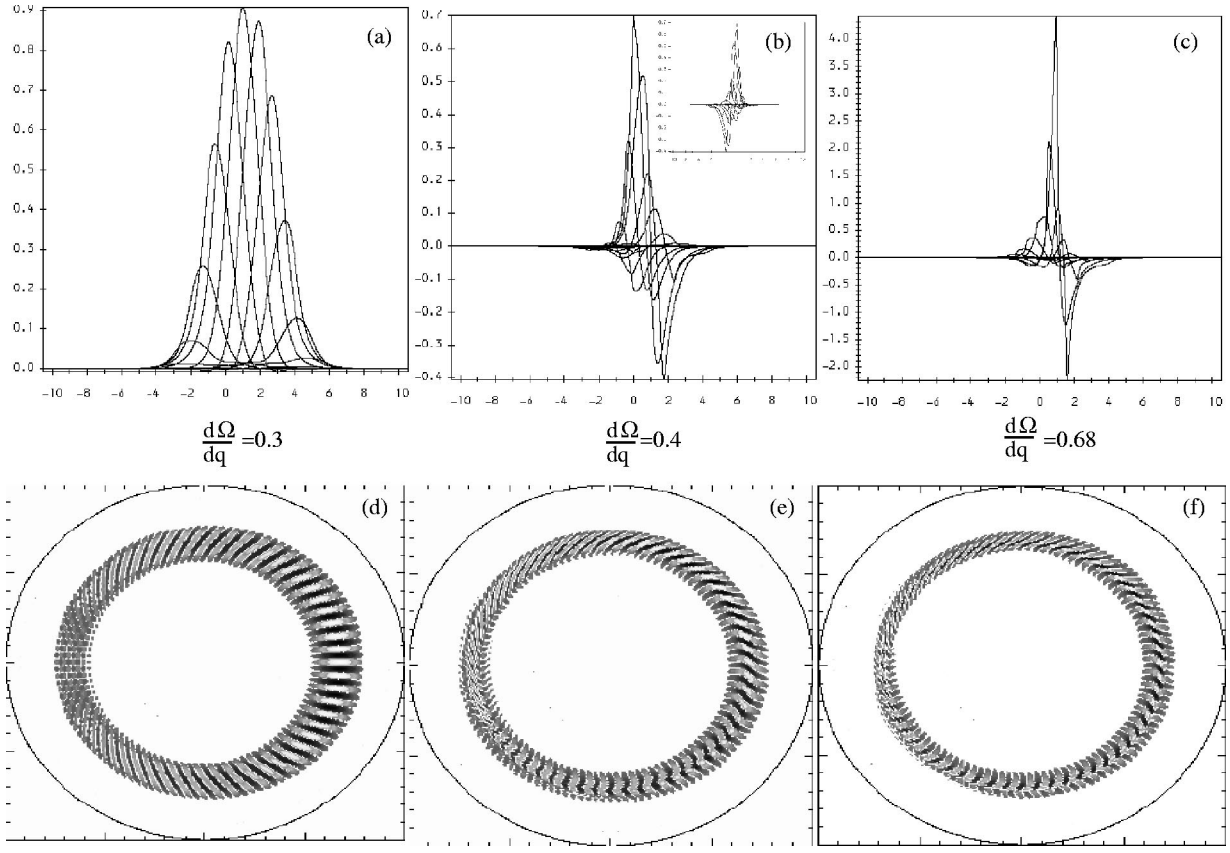

FIG. 6. $s=1$, $\alpha=2$, $\Lambda=1.35$: (a)–(c) Plots of the individual Fourier mode amplitudes $u_m(x)$, for different values of the flow shear. (d)–(f) The amplitude of the perturbations in poloidal cross section. (b) and its inset show the mirror-symmetric mode structures of the two complex-conjugate solutions that exist at higher flow shears.

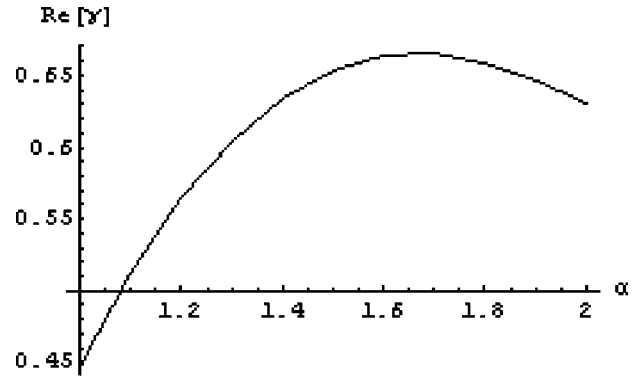

FIG. 7. $s=1$, zero flow shear. The most unstable γ is for $\alpha \simeq 1.7$. (The calculation was done for $\Lambda = 2.62$.)

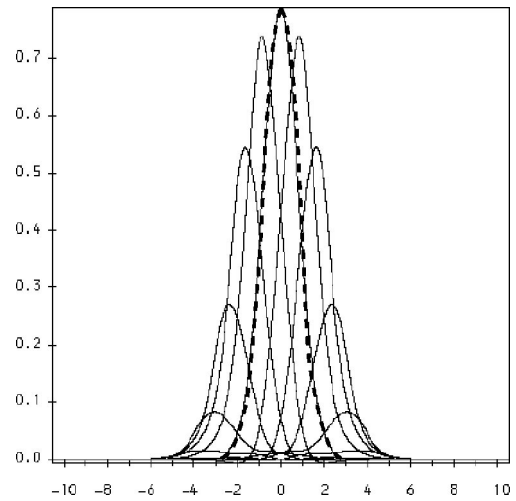

FIG. 8. $s=1$, $\alpha=2$, $\Lambda=1.35$, zero flow-shear. The central Fourier mode (dashed line) extends well beyond the most unstable radial positions at $x = \pm 1$, so the mode centers on $x=0$.

for $\alpha(x)$, with $\alpha(x)=\alpha_0 \exp(-x^2/2s^2\Lambda^4)$. So for $s=1$, $\alpha_0 = 2$ the most unstable radial positions have $\alpha(x) \simeq 1.7$, and are at $x=x^* \simeq \pm \Lambda^2 \sqrt{2 \ln(2/1.7)}$. For $\Lambda = 1.35$ this gives $x^* = \pm 1.0$, but Fig. 8 shows that the central Fourier mode extends well beyond $x = \pm 1$, and hence the radial structure remains centred on $x=0$. However for $\Lambda = 2.62$, $x^* = \pm 3.9$, and Fig. 9 shows that the mode then peaks at the most unstable radial positions of $x^* = \pm 3.9$.

Figures 3 and 6 indicate that flow shear will narrow the mode envelope. Therefore at sufficiently high flow shears, the mode will no longer be able to extend beyond $\pm x^*$, and must instead center on $+x^*$ or $-x^*$. This is confirmed for $\Lambda = 1.35$ in Fig. 6, that shows the complex-conjugate solutions centering on $x^* = \pm 1.0$. If the mode subsequently rotates with the flow at $x=x^*$, then Eqs. (13) and (14) tell us that $\mathrm{Im}(\gamma) = \pm (d\Omega/dq) x^*$, which to a good approximation is the case [Fig. 2(b)].

In summary, the loss of mode symmetry is because the mode wants to localise in the most unstable radial position. For $s=1.0$ and $\alpha=2.0$, there are two such positions at $x = \pm x^*$. The flow shear *narrows* the mode, so that it is no longer able to extend across *both* of these positions, and must instead sit at *either* $x = +|x^*|$ or $x = -|x^*|$. The complex conjugate solutions arise because the mode wants to rotate with the flow (introducing an imaginery component), and there are two equivalent, equally unstable positions at which the mode can localize.

The above argument suggests that closer to marginal stability (where there will be a single position of maximum instability, at $x=0$), that the mode structures should remain symmetric and the growth rate real. This was confirmed by calculations at $s=1.0$ and $\alpha=1.0$ for $\Lambda = 1.35$ (see Fig. 10), for which there is no longer any coupling of different solution branches, the growth rate is always real, and the mode structures remain symmetric throughout. However, equivalent calculations with $\Lambda = \infty$ showed that γ was no longer a monotonically decreasing function of $d\Omega/dq$, and became unstable again in the region of $0.6 \lesssim d\Omega/dq \lesssim 0.9$. A number of similar calculations for $s=1.0$ and $\Lambda = \infty$ are summarized in Fig. 11. For $\alpha \gtrsim 1$, increasing the flow shear $d\Omega/dq$ would

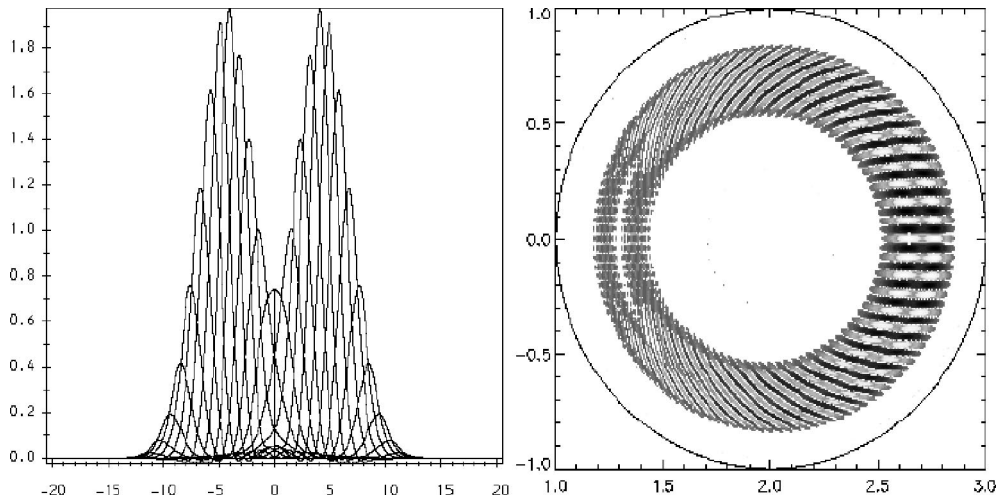

FIG. 9. $s=1$, $\alpha=2$, $\Lambda=2.62$, zero flow shear. The most unstable radial positions are at $x \simeq \pm 4$, well beyond the width of individual Fourier modes. Hence the mode peaks at $x \simeq \pm 4$. The Fourier mode amplitudes $u_m(x)$ are shown on the left of the figure, and the mode amplitude in poloidal cross section is on the right.

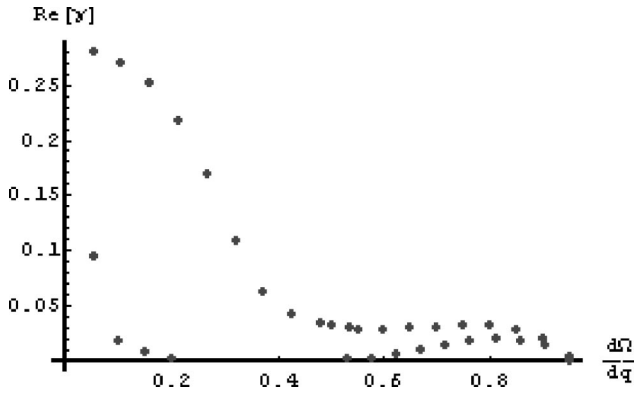

FIG. 10. $s=1$, $\alpha=1$: $\Lambda=1.35$ (small circles), $\Lambda=\infty$ (large circles). For $\Lambda=\infty$ the mode stabilizes, then is destabilized again for $d\Omega/dq\simeq 0.5$, before finally stabilizing again.

stabilize a previously unstable mode (as expected). However for smaller values of $\alpha\sim 0.5$, increasing the flow shear could *destabilize* a previously *stable* mode. The mechanism by which this occurs is the subject of ongoing work.

Finally we consider what realistic values of the flow shear are required to stabilize ballooning modes. We take an ITB width Δr, a minor radius r, a change in flow speed Δv over an ITB, and an Alfvén speed v_A. Ω is normalized such that $\Omega\rightarrow(\Omega Rq/c_s)\sqrt{p/B^2}=\Omega Rq/v_A$, so taking flow shear to be important for $d\Omega/dq\gtrsim 1$ requires $1\lesssim(Rq/v_A)\times(d\Omega/dq)=(R/v_A)(r/s)(d\Omega/dr)$. Writing $\Delta v=Rd\Omega$ and $\Delta r=dr$, then flow shear will be important when

$$\Delta v\gtrsim v_A s\frac{\Delta r}{r}$$

indicating a critical magnetic shear below which flow shear will be important for ballooning mode stability.

V. CONCLUSIONS

We have used an eigenmode (as opposed to ''eikonal'') approach to study ballooning modes in the presence of flow shear, applying it to a simple circular flux-surfaces model of ITBs. In the absence of flow shear, we find that at sufficiently low *magnetic* shear, the equilibrium α profile has a negligible effect on the mode structure, and our results are in good agreement with analytic calculations in this limit.

Flow shear can stabilize ballooning modes, but the structure and stability of ballooning modes may be significantly different when the effect of weak equilibrium variations are included. The extent to which the equilibrium *profile* may affect ballooning modes, is incorporated into a parameter $\Lambda\equiv\sqrt{nq/a}$, that for zero flow-shear, characterizes the mode envelope's width in x-space. At low flow-shears the growth rate is significantly greater for finite $\Lambda=\sqrt{nq/a}$ than for $\Lambda=\infty$, but the growth rate tends to that of $\Lambda=\infty$ as the flow shear is increased.

When $\Lambda=\infty$, the growth rates remain real, and the mode structures symmetric for all values of the flow shear $d\Omega/dq$. This contrasts with finite Λ, for which sufficiently unstable ballooning modes can develop a radially asymmetric structure and the growth rate become complex. This behavior is explained in terms of the flow shear narrowing the mode envelope, the radially dependent stability of the zero flow-shear equilibrium, the mode's desire to localize at the most unstable radial position, and the mode's desire to rotate with the equilibrium flow. Nearer to marginal stability, with $s=1$, $\alpha\lesssim 0.5$, and $\Lambda=\infty$, we find that (in addition to being able to stabilize an unstable ballooning mode), flow shear can drive a previously stable mode unstable.

Finally we note that flow-shear is expected to be important for a change in flow speed Δv over an ITB width Δr, for which $\Delta v\sim v_A s\Delta r/r$. So for a given $\Delta r/r$ and $\Delta v/v_A$, there will be a critical magnetic shear below which flow shear will be important for stabilizing ballooning modes. This suggests that flow shear is likely to be important for the stability of ITBs, which are typically associated with low s.

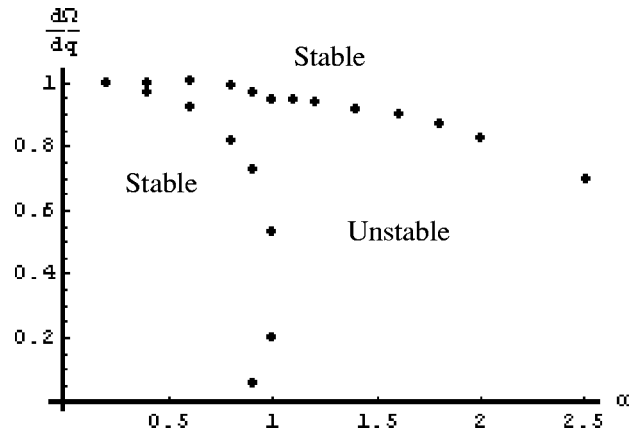

FIG. 11. $s=1$, $\Lambda=\infty$: Plotting α against $d\Omega/dq$ indicates that in addition to flow shear stabilizing unstable modes (for $\alpha\gtrsim 1$), flow shear can also destabilize previously stable modes ($\alpha\lesssim 1$). Boundary points shown are for when $\mathrm{Re}(\gamma)$ falls to $\mathrm{Re}(\gamma)\lesssim 0.002$.

ACKNOWLEDGMENTS

Thanks to Jack Connor, Jim Hastie, and Bryan Taylor for useful discussions.

This work was jointly funded by the United Kingdom Engineering and Physical Sciences Research Council, and EURATOM.

[1] J.P. Freidberg, *Ideal Magneto-Hydro-Dynamics* (Plenum, New York, 1987), p. 364.
[2] J.W. Connor, R.J. Hastie, and J.B. Taylor, Phys. Rev. Lett. **40**, 396 (1978).
[3] J.W. Connor, R.J. Hastie, and J.B. Taylor, Proc. R. Soc. London, Ser. A **365**, 1 (1979).
[4] R.L. Dewar and A.H. Glasser, Phys. Fluids **26**, 3038 (1983).
[5] J.M. Greene and M.S. Chance, Nucl. Fusion **21**, 453 (1981).
[6] J. Wesson, *Tokamaks* (Oxford University Press, Oxford, 1997), p. 313.
[7] R.C. Wolf, Plasma Phys. Controlled Fusion **45**, R1 (2003).
[8] W.A. Cooper, Plasma Phys. Controlled Fusion **30**, 1805 (1988).
[9] R.L. Miller, F.L. Waelbroeck, A.B. Hassam *et al.*, Phys. Plasmas **2**, 3676 (1995).
[10] M. Furukawa, Y. Nakamura, S. Hamaguchi *et al.*, Phys. Plasmas **8**, 4889 (2001).
[11] A.J. Webster and H.R. Wilson, in *Proceedings of the Joint Varenna-Lausanne International Workshop on Theory of Fusion Plasmas*, Varenna, Italy, 2002, edited by J.W. Connor, O. Sauter, and E. Sindoni (Societa Italiana di Fisica, Bologna, Italy, 2002), Vol. 20, p. 417.
[12] Flow shear is found to radially confine the mode, even for $\Lambda=n=\infty$. So it is straightforward to study $n=\infty$ when the flow shear is nonzero.

[13]T.J. Martin, Developed at UKAEA/EURATOM Fusion Association, Culham Science Centre, Abingdon, OX14 3DB, United Kingdom.
[14]J.W. Connor and R.J. Hastie, ''Stability of internal transport barriers to ideal MHD ballooning modes,'' Phys. Rev. Lett. (to be published).
[15]F.L. Waelbroeck and L. Chen, Phys. Fluids B **3**, 601 (1991).
[16]The reduction in the growth rate for larger values of α corresponds to passing through the $s-\alpha$ stability diagram toward the region of ''second stability'' (Ref. 1).